Segmented Reconstruction of Low-Acceleration Orbital Maneuvers

Oliver Jia-Richards*
University of Michigan, Ann Arbor, Michigan 48109

This paper considers the problem of inferring the acceleration acting on a spacecraft in a near-circular orbit around a large planetary body when the acceleration is known to act in the along-track direction. A segmented approach is analyzed where the acceleration profile over a given period of time is approximated as a piecewise-constant profile. Noisy measurements of the spacecraft's position are collected throughout the acceleration profile, from which the constant acceleration for each segment of the piecewise-constant profile can be inferred. The primary contribution of this work is an analytical approximation for the sensitivity of each measurement with respect to the constant acceleration of each segment. The resulting analytically-approximated sensitivity matrix enables an analytical reconstruction of the acceleration profile given a numerically-simulated reference trajectory. Applications of the segmented approach for thrust inference for both discontinuous and continuous thrust profiles are demonstrated. In particular, the reconstruction of a simulated thruster degradation profile over the course of sixty hours is shown.

I. Introduction

The ability to characterize the thrust output of a propulsion system in space is a critical capability for the final stages of propulsion system development as well as monitoring the thruster's behavior during operations. Of particular difficulty is thrust estimation for low-thrust propulsion systems such as electric propulsion and micro-propulsion systems where the resulting propulsive acceleration may be too low ($\sim$1 μm/s^2) for measurement by onboard accelerometers. Instead, low-thrust estimation relies on using the propulsion system to produce a force or torque on the parent spacecraft and inferring the thrust output based on the dynamic response of the spacecraft. In the case of using the thruster to produce a force, the spacecraft performs an orbital maneuver, such as an orbit raising maneuver by aligning the thrust vector in the along-track direction. In the case of using the thruster to produce a torque, the spacecraft performs an attitude maneuver. The thrust output of the propulsion system can then be inferred based on an estimate of the observed change in spacecraft attitude or attitude rates as well as the estimated lever arm of the thruster.

The Space Electric Rocket Test (SERT) missions were the first missions to demonstrate in-space thrust estimation techniques for low-acceleration propulsion systems using both orbital and attitude maneuvers. SERT I configured the propulsion system to produce torques on the spacecraft and estimated thrust based on the change in the spacecraft's spin rate [1]. Alternatively, SERT II configured the propulsion system such that the propulsive acceleration had an along-track component and estimated thrust based on the change in the spacecraft's orbital radius [2]. Both SERT I and SERT II carried on-board accelerometers in order to take instantaneous measurements of the acceleration produced by their respective propulsion systems. However, the use of an on-board accelerometer with sufficient precision to measure low ($\sim$1 μm/s^2) propulsive accelerations for a scientific mission may be a luxury. This is particularly true for small spacecraft where such accelerometers may take up a significant portion of the spacecraft mass and volume budget [3].

The application and analysis of attitude maneuvers for in-space thrust estimation has been under frequent consideration. The Mars Cube One spacecraft performed in-space thrust estimation by measuring the total change in angular momentum of the spacecraft [4]. In a similar procedure, the thrusters onboard Cassini were calibrated during measured flight telemetry during reaction wheel biasing [5]. The University Würzburg Experimental satellite–4 also demonstrated the use of attitude control maneuvers to measure the thrust magnitude as well as direction for multiple onboard thrusters [6]. Developments in the use of attitude control maneuvers for thrust estimation continue to be made, such as the inclusion of angular velocity periodicity in the thrust estimation in order to improve thrust estimation in the presence of noisy measurements [7]. Methods combining attitude maneuvers and small position maneuvers have also been considered [8].

*Assistant Professor, Department of Aerospace Engineering, oliverjr@umich.edu, Member AIAA

While methods for thrust estimation based on attitude maneuvers have demonstrated success for in-space thrust estimation, such methods are not always applicable and may face significant uncertainty when applied on small spacecraft. In order to perform an attitude maneuver, the thrust vector must be offset from the spacecraft center of mass such that the propulsion system can produce a torque. For spacecraft that carry only a single thruster, such an offset is undesired and precludes the use of attitude maneuvers for thrust estimation. In addition, in order to estimate the thrust of the propulsion system, the lever arm of the propulsion system needs to be known. For small spacecraft the lever arm of the propulsion system may be on the order of a few centimeters. As such, uncertainty in the thruster lever arm of only a few millimeters would lead to 10% uncertainty in the thrust estimate. Uncertainty in the thruster lever arm can come from a number of sources, including the thruster itself. For thrusters such as ionic-liquid electrospray thrusters which are based on an array of individual emitters, spatial variation of emission across the array [9, 10] could lead to uncertainties in the thruster lever arm of a few millimeters or more.

The development of propulsion systems for small spacecraft is also an extremely active research area; many low-thrust propulsion systems for small spacecraft such as ionic-liquid electrospray thrusters [11, 12], film-evaporating water microcapillaries [13], miniaturized ion thrusters [14], and plasma thrusters [15, 16] are actively under development and will likely have in-space demonstrations in the near future. As such, the development of thrust estimation methods that leverage orbital maneuvers is desired as they can be applied to a wider range of missions and avoid uncertainties associated with the thruster lever arm for small spacecraft. One of the simplest approaches for low-thrust estimation based on orbital maneuvers is to perform an orbit raise for a near-circular orbit. Simple analytical approximations for estimating the thrust based on the initial and final orbital radius of the spacecraft exist, and were leveraged for the SERT II mission [2], and continue to be used for recent in-space demonstrations of electric propulsion systems in order to provide a rough verification of the propulsion system thrust output [17–19].

Numerical approaches for thrust estimation based on orbital maneuvers have also seen recent development. However, many of the methods are not necessarily targeted at general thrust characterization and instead consider problems with certain limitations. Methods that target maneuver detection for an uncooperative spacecraft that performs maneuvers at an unknown time [20, 21] or when telemetry may not be available during the maneuver [22, 23] often leverage filtering which limits the reconstruction of earlier portions of the propulsion system thrust and may not efficiently use all available information. As such, methods directly targeted at thrust estimation for cooperative spacecraft based on iterative batch filters [24] or the ensemble Kalman update [25] have also been analyzed and both show promising results.

This paper again targets the question of thrust estimation based on orbital maneuvers for cooperative spacecraft, but takes a different approach from the prior numerical methods. Both Refs. [24] and [25] require the use of multiple numerical simulations of the spacecraft trajectory—either for each iteration of the batch filter [24] or to estimate the optimal Kalman gain with ensemble approaches [25]—which can be computationally expensive, especially for high-fidelity models. Instead, this paper takes a more analytical approach to the thrust inference problem where only a single simulation of the spacecraft trajectory is required as a reference for a linear update to the propulsive acceleration profile. In addition, instead of estimating only a single average propulsive acceleration, a segmented reconstruction is considered where time-varying propulsive accelerations can be represented as a piecewise-constant profile. This is accomplished by deriving analytical approximations for the sensitivity of the spacecraft position with respect to the acceleration magnitude of each segment of the piecewise-constant profile.

As a result, this paper develops a method that can be used to approximately reconstruct time-varying propulsive accelerations based on orbital maneuvers where the spacecraft is assumed to be in a near-circular orbit and the propulsive acceleration vector is assumed to be aligned in the along-track direction. The method is demonstrated on both discontinuous acceleration profiles, such as thruster startup, and continuous acceleration profiles, such as thruster degradation. In particular, the ability to reconstruct a sixty hour acceleration profile for a thruster undergoing thrust degradation due to propellant depletion is demonstrated. The method can be generally applied to any accelerations that act in the along-track direction which includes propulsive accelerations for orbit-raising maneuvers as well as atmospheric drag for near-circular orbits.

II. Problem Statement

The problem addressed in this work is the inference of a spacecraft's initial state as well as a piecewise-constant along-track acceleration profile from noisy measurements of a spacecraft's position. Specifically, given a vector of k

measurement times,

$$\tau = \begin{bmatrix} t_1 & \dots & t_k \end{bmatrix}^T \tag{1}$$

it is assumed that a measurement of the spacecraft's full position is provided in an inertial planetocentric frame (e.g. an Earth-centered inertial frame). Note, there is no requirement that the measurement times be ordered chronologically, but it typically will be. The measurement vector then contains $3k$ elements corresponding to the x, y, and z position of the spacecraft at each measurement time

$$m = \begin{bmatrix} x(t_1) & y(t_1) & z(t_1) & \dots & x(t_k) & y(t_k) & z(t_k) \end{bmatrix}^T \tag{2}$$

with corresponding covariance matrix Σ_m.

The desired parameter vector contains the initial spacecraft state as well as the acceleration magnitudes for a piecewise-constant representation of the along-track acceleration applied to the spacecraft throughout observed measurement duration

$$\phi = \begin{bmatrix} x(t_0) & y(t_0) & z(t_0) & v_x(t_0) & v_y(t_0) & v_z(t_0) & \alpha_1 & \dots & \alpha_q \end{bmatrix}^T \tag{3}$$

where t_0 is the initial time of the maneuver and α_1 through α_q represent the acceleration magnitude for an q-segment piecewise-constant representation of the along-track acceleration acting on the spacecraft. It is worth noting that each α_i represents the total along-track acceleration acting on the spacecraft, which is inclusive of both propulsive acceleration and atmospheric drag acceleration as the spacecraft is assumed to be in a near-circular orbit. For each segment a time interval, Δt_i, can be defined over which a constant along-track acceleration of α_i acts on the spacecraft. The length of the time interval is allowed to vary between time segments. In this work it is assumed that segments are sequentially applied such that the end time of segment i ($i < q$) is equal to the start time of segment $i + 1$. As such, the overall length of the maneuver is

$$T = \sum_{i=1}^{q} \Delta t_i \tag{4}$$

The prior covariance matrix for the parameter vector is defined to be the matrix Σ_ϕ.

Given a particular parameter vector as well as a gravitational field model for the planet of interest, it is relatively simple to numerically simulate the corresponding measurement vector. The goal of this work is to infer a parameter vector from an observed measurement vector in a linear manner. However, instead of working with the original inertial representation of the initial state and measurements, deviations in the parameter vector as well as measurement residuals will be considered in a local-vertical, local-horizontal frame. Assume at a particular time, t, the spacecraft has an inertial position, $[x(t), y(t), z(t)]$, and velocity, $[v_x(t), v_y(t), v_z(t)]$. First, define the radial unit vector

$$\hat{r}(t) = \frac{1}{\sqrt{x(t)^2 + y(t)^2 + z(t)^2}} \begin{bmatrix} x(t) \\ y(t) \\ z(t) \end{bmatrix} \tag{5}$$

and velocity unit vector

$$\hat{v}(t) = \frac{1}{\sqrt{v_x(t)^2 + v_y(t)^2 + v_z(t)^2}} \begin{bmatrix} v_x(t) \\ v_y(t) \\ v_z(t) \end{bmatrix} \tag{6}$$

Next define the cross-track unit vector

$$\hat{c}(t) = \frac{\hat{r}(t) \times \hat{v}(t)}{\|\hat{r}(t) \times \hat{v}(t)\|} \tag{7}$$

and along-track unit vector

$$\hat{a}(t) = \hat{c}(t) \times \hat{r}(t) \tag{8}$$

The local-vertical, local-horizontal frame at a given time is then defined by the unit vectors $\{\hat{r}(t), \hat{a}(t), \hat{c}(t)\}$. The rotation matrix from the inertial frame to the local-vertical, local-horizontal frame is then

$$R(t) = \begin{bmatrix} \hat{r}(t)^T \\ \hat{a}(t)^T \\ \hat{c}(t)^T \end{bmatrix} \tag{9}$$

Given deviations in the initial spacecraft position and velocity from the expected values, $[\Delta x(t_0), \Delta y(t_0), \Delta z(t_0)]$ and $[\Delta v_x(t_0), \Delta v_y(t_0), \Delta v_z(t_0)]$, define the deviations in the local-vertical, local-horizontal frame

$$\begin{bmatrix} \Delta r(t_0) \\ \Delta a(t_0) \\ \Delta c(t_0) \end{bmatrix} = R(t_0) \begin{bmatrix} \Delta x(t_0) \\ \Delta y(t_0) \\ \Delta z(t_0) \end{bmatrix} \tag{10}$$

and

$$\begin{bmatrix} \Delta v_r(t_0) \\ \Delta v_a(t_0) \\ \Delta v_c(t_0) \end{bmatrix} = R(t_0) \begin{bmatrix} \Delta v_x(t_0) \\ \Delta v_y(t_0) \\ \Delta v_z(t_0) \end{bmatrix} \tag{11}$$

where the rotation matrix is given by Eq. 9. Now define deviations in an alternate parameter vector, $\tilde{\phi}$, where the position and velocity vectors are taken in the local-vertical, local-horizontal frame

$$\Delta\tilde{\phi} = \begin{bmatrix} \Delta r(t_0) & \Delta s(t_0) & \Delta c(t_0) & \Delta v_r(t_0) & \Delta v_s(t_0) & \Delta v_c(t_0) & \Delta\alpha_1 & \dots & \Delta\alpha_q \end{bmatrix}^T \tag{12}$$

The covariance matrix for the alternate parameter vector is given by

$$\tilde{\Sigma}_\phi = R_\phi \Sigma_\phi R_\phi^T \tag{13}$$

where

$$R_\phi = \begin{bmatrix} R(t_0) & 0_3 & 0_{3\times q} \\ 0_3 & R(t_0) & 0_{3\times q} \\ 0_{q\times 3} & 0_{q\times 3} & I_q \end{bmatrix} \tag{14}$$

and 0_3 is a 3×3 zero matrix, $0_{3\times q}$ is a $3 \times q$ zero matrix, $0_{q\times 3}$ is a $q \times 3$ zero matrix, and I_q is a $q \times q$ identity matrix.

Similarly, deviations in the measurement vector need to be redefined to be in the local-vertical, local-horizontal frame. Given a numerical simulation, represented as a vector function $f(t, \phi)$, that can take the expected value of the parameter vector and simulate measurements at the desired measurement times

$$\begin{bmatrix} \hat{x}(t) \\ \hat{y}(t) \\ \hat{z}(t) \end{bmatrix} = f(t, \phi) \tag{15}$$

calculate the error between the simulated measurements and observed measurements at each measurement time

$$\begin{bmatrix} \Delta x(t) \\ \Delta y(t) \\ \Delta z(t) \end{bmatrix} = \begin{bmatrix} x(t) \\ y(t) \\ z(t) \end{bmatrix} - f(t, \phi) \tag{16}$$

Finally, rotate the position errors into the local-vertical, local-horizontal frame with the rotation matrix calculated from Eq. 9 using the simulated measurements

$$\begin{bmatrix} \Delta r(t) \\ \Delta a(t) \\ \Delta c(t) \end{bmatrix} = R(t) \begin{bmatrix} \Delta x(t) \\ \Delta y(t) \\ \Delta z(t) \end{bmatrix} \tag{17}$$

The deviations in the alternate measurement vector are then simply the deviations in the radial, along-track, and cross-track position evaluated at the desired measurement times

$$\Delta\tilde{m} = \begin{bmatrix} \Delta r(t_1) & \Delta a(t_1) & \Delta c(t_1) & \dots & \Delta r(t_k) & \Delta a(t_k) & \Delta c(t_k) \end{bmatrix}^T \tag{18}$$

The covariance matrix for the alternate measurement vector is given by

$$\tilde{\Sigma}_m = R_m \Sigma_m R_m^T \tag{19}$$

where

$$R_m = \begin{bmatrix} R(t_1) & 0_3 & \dots & 0_3 \\ 0_3 & R(t_2) & \dots & 0_3 \\ \vdots & \vdots & \ddots & \vdots \\ 0_3 & 0_3 & \dots & R(t_k) \end{bmatrix} \tag{20}$$

Given deviations in the alternate parameter and measurement vectors, the goal of this work is to determine a linear relationship between the two vectors

$$\Delta\tilde{m} = H\Delta\tilde{\phi} \tag{21}$$

Specifically, the goal is to analytically approximate the sensitivity matrix, H. The sensitivity matrix will be a $(3k)\times(q+6)$ matrix describing the sensitivity of each measurement with respect to each parameter

$$H = \begin{bmatrix} \frac{\partial r}{\partial r_0}(t_1) & \frac{\partial r}{\partial a_0}(t_1) & \frac{\partial r}{\partial c_0}(t_1) & \frac{\partial r}{\partial v_{r,0}}(t_1) & \frac{\partial r}{\partial v_{a,0}}(t_1) & \frac{\partial r}{\partial v_{c,0}}(t_1) & \frac{\partial r}{\partial \alpha_1}(t_1) & \dots & \frac{\partial r}{\partial \alpha_q}(t_1) \\ \frac{\partial a}{\partial r_0}(t_1) & \frac{\partial a}{\partial a_0}(t_1) & \frac{\partial a}{\partial c_0}(t_1) & \frac{\partial a}{\partial v_{r,0}}(t_1) & \frac{\partial a}{\partial v_{a,0}}(t_1) & \frac{\partial a}{\partial v_{c,0}}(t_1) & \frac{\partial a}{\partial \alpha_1}(t_1) & \dots & \frac{\partial a}{\partial \alpha_q}(t_1) \\ \frac{\partial c}{\partial r_0}(t_1) & \frac{\partial c}{\partial a_0}(t_1) & \frac{\partial c}{\partial c_0}(t_1) & \frac{\partial c}{\partial v_{r,0}}(t_1) & \frac{\partial c}{\partial v_{a,0}}(t_1) & \frac{\partial c}{\partial v_{c,0}}(t_1) & \frac{\partial c}{\partial \alpha_1}(t_1) & \dots & \frac{\partial c}{\partial \alpha_q}(t_1) \\ \vdots & \vdots & \vdots & \vdots & \vdots & \vdots & \vdots & & \vdots \\ \frac{\partial r}{\partial r_0}(t_k) & \frac{\partial r}{\partial a_0}(t_k) & \frac{\partial r}{\partial c_0}(t_k) & \frac{\partial r}{\partial v_{r,0}}(t_k) & \frac{\partial r}{\partial v_{a,0}}(t_k) & \frac{\partial r}{\partial v_{c,0}}(t_k) & \frac{\partial r}{\partial \alpha_1}(t_k) & \dots & \frac{\partial r}{\partial \alpha_q}(t_k) \\ \frac{\partial a}{\partial r_0}(t_k) & \frac{\partial a}{\partial a_0}(t_k) & \frac{\partial a}{\partial c_0}(t_k) & \frac{\partial a}{\partial v_{r,0}}(t_k) & \frac{\partial a}{\partial v_{a,0}}(t_k) & \frac{\partial a}{\partial v_{c,0}}(t_k) & \frac{\partial a}{\partial \alpha_1}(t_k) & \dots & \frac{\partial a}{\partial \alpha_q}(t_k) \\ \frac{\partial c}{\partial r_0}(t_k) & \frac{\partial c}{\partial a_0}(t_k) & \frac{\partial c}{\partial c_0}(t_k) & \frac{\partial c}{\partial v_{r,0}}(t_k) & \frac{\partial c}{\partial v_{a,0}}(t_k) & \frac{\partial c}{\partial v_{c,0}}(t_k) & \frac{\partial c}{\partial \alpha_1}(t_k) & \dots & \frac{\partial c}{\partial \alpha_q}(t_k) \end{bmatrix} \tag{22}$$

Assuming an approximation of the sensitivity matrix can be found, the expected value and covariance of the parameter vector can be updated according to

$$\Delta\bar{\phi} = \Delta\bar{\phi} + K\Delta\tilde{m} \tag{23}$$

and

$$\tilde{\Sigma}_\phi = (I_{q+6} - KH)\tilde{\Sigma}_\phi \tag{24}$$

where I_{q+6} is a $(q+6)\times(q+6)$ identity matrix and K is the optimal Kalman gain calculated as

$$K = \tilde{\Sigma}_\phi H^T \left(H\tilde{\Sigma}_\phi H^T + \tilde{\Sigma}_m \right)^{-1} \tag{25}$$

which allows the acceleration magnitude of each segment of the piecewise-constant representation of the acceleration profile to be inferred.

Assuming that the initial spacecraft orbit is near-circular, the first six columns of the sensitivity matrix—corresponding to the sensitivity of the measurements with respect to the initial spacecraft state in a local-vertical, local-horizontal frame—are directly given by linear orbit theory [26]

$$\begin{bmatrix} \Delta r(t) \\ \Delta a(t) \\ \Delta c(t) \end{bmatrix} \approx \begin{bmatrix} 4-3\cos(nt) & 0 & 0 & \frac{1}{n}\sin(nt) & \frac{2}{n}(1-\cos(nt)) & 0 \\ 6(\sin(nt)-nt) & 1 & 0 & -\frac{2}{n}(1-\cos(nt)) & \frac{1}{n}(4\sin(nt)-3nt) & 0 \\ 0 & 0 & \cos(nt) & 0 & 0 & \frac{1}{n}\sin(nt) \end{bmatrix} \begin{bmatrix} \Delta r_0 \\ \Delta a_0 \\ \Delta c_0 \\ \Delta v_{r,0} \\ \Delta v_{a,0} \\ \Delta v_{c,0} \end{bmatrix} \tag{26}$$

where n is the mean motion of the spacecraft's initial orbit. By evaluating these sensitivities at the desired measurement times, the first six columns of the sensitivity matrix can be formed. The contribution of this work is determining approximations for the sensitivity of the spacecraft position in a local-vertical, local-horizontal frame due to a segmented along-track acceleration profile.

III. Trajectory Approximation

In order to determine approximations for the sensitivity of the spacecraft position in a local-vertical, local-horizontal frame due to a segmented along-track acceleration profile, the first step will be to determine an analytical approximation for the spacecraft's overall trajectory. The specific energy of a spacecraft's orbit, ϵ, is given by

$$\epsilon = \frac{1}{2}v^2 - \frac{\mu}{r} \tag{27}$$

where v is the speed of the spacecraft, μ is the gravitational parameter of the central body, and r is the radial position of the spacecraft. Assuming that the orbit is circular, then the specific energy can be written as a function of only the orbital radius

$$\epsilon = -\frac{1}{2}\frac{\mu}{r} \tag{28}$$

The time derivative of the specific energy, the specific power, is therefore

$$\frac{d\epsilon}{dt} = \frac{1}{2}\frac{\mu}{r^2}\frac{dr}{dt} \tag{29}$$

If the spacecraft carries a propulsion system that produces a constant propulsive acceleration, α, and assuming that the propulsive acceleration is aligned with the spacecraft's velocity vector, then the specific power input to the spacecraft's orbit from the propulsion system is given by

$$p = \alpha v = \alpha\sqrt{\frac{\mu}{r}} \tag{30}$$

Assuming that the only power input to the spacecraft's orbit comes from its propulsion system, then Eqs. 29 and 30 can be equated to give an ordinary differential equation for the orbital radius

$$\frac{dr}{dt} = \frac{2\alpha}{\sqrt{\mu}}r^{3/2} \tag{31}$$

This differential equation can be analytically integrated to give an approximation for the orbital radius as a function of time

$$r(t) = r_0\left(1 - \frac{\alpha}{\sqrt{\mu/r_0}}t\right)^{-2} \tag{32}$$

where r_0 is the initial orbital radius. From the approximation of the spacecraft's radial position over time, the angular position of the spacecraft in the orbital plane can also be approximated

$$\theta(t) = \theta_0 + \int_0^t \sqrt{\frac{\mu}{r^3(\tau)}}d\tau \tag{33}$$

$$= \theta_0 + \frac{1}{4}\frac{\mu}{\alpha r_0^2}\left[1 - \left(1 - \frac{\alpha}{\sqrt{\mu/r_0}}t\right)^4\right] \tag{34}$$

where θ_0 is the initial angular position. This approximation of the spacecraft's radial and angular position within the orbital plane is well known and has been presented previously [27]. However, it is limited to a single propulsive acceleration that acts for the entire duration of time.

In order to account for a segmented acceleration profile, the trajectory approximation will need to be extended. Assume that the acceleration profile is broken into two segments: α_1 which acts on the time range $t \in [0, \Delta t_1)$ and α_2 which acts in the time range $t \in [\Delta t_1, \Delta t_1 + \Delta t_2)$. Over the time range $t \in [0, \Delta t_1)$ the radial position of the spacecraft can be approximated with Eq. 32 and substituting in α_1 for the along-track acceleration

$$r_1(t) = r_0 \left(1 - \frac{\alpha_1}{\sqrt{\mu/r_0}} t\right)^{-2} \qquad t \in [0, \Delta t_1) \tag{35}$$

Over the time range $t \in [\Delta t_1, \Delta t_1 + \Delta t_2)$ the along-track acceleration magnitude changes to α_2. Continuing the approximation that the spacecraft's orbit is near-circular, then the radial position of the spacecraft can be approximated from

$$r_2(t) = r_0' \left(1 - \frac{\alpha_2}{\sqrt{\mu/r_0'}} (t - \Delta t_1)\right)^{-2} \qquad t \in [\Delta t_1, \Delta t_1 + \Delta t_2) \tag{36}$$

where the initial radial position, r_0', is given by the radial position of the spacecraft at the end of the first segment

$$r_0' = r_1(\Delta t_1) = r_0 \left(1 - \frac{\alpha_1}{\sqrt{\mu/r_0}} \Delta t_1\right)^{-2} \tag{37}$$

which results in

$$r_2(t) = r_0 \left(1 - \frac{\alpha_1}{\sqrt{\mu/r_0}} \Delta t_1 - \frac{\alpha_2}{\sqrt{\mu/r_0}} (t - \Delta t_1)\right)^{-2} \qquad t \in [\Delta t_1, \Delta t_1 + \Delta t_2) \tag{38}$$

This process can be extended to an arbitrary number of segments. For a particular segment, i, the approximation for the radial position during the segment will be given by

$$r_i(t) = r_0 \left(1 - \frac{\Delta v_{1:i-1}}{\sqrt{\mu/r_0}} - \frac{\alpha_i}{\sqrt{\mu/r_0}} (t - T_{i-1})\right)^{-2} \qquad t \in [T_{i-1}, T_{i-1} + \Delta t_i) \tag{39}$$

where

$$\Delta v_{1:i-1} = \sum_{j=1}^{i-1} \alpha_j \Delta t_j \tag{40}$$

and

$$T_{i-1} = \sum_{j=1}^{i-1} \Delta t_j \tag{41}$$

From the approximation of the radial position, the angular position of the spacecraft during segment i can be approximated from

$$\theta_i(t) = \theta_{0,i} + \int_{T_{i-1}}^{T_{i-1}+\Delta t_i} \sqrt{\frac{\mu}{r^3(\tau)}} d\tau \tag{42}$$

$$= \theta_{0,i} + \frac{1}{4} \frac{\mu}{r_0^2 \alpha_i} \left[\Gamma_i^4 - \left(\Gamma_i - \frac{\alpha_i}{\sqrt{\mu/r_0}} (t - T_{i-1})\right)^4\right] \qquad t \in [T_{i-1}, T_{i-1} + \Delta t_i) \tag{43}$$

where

$$\Gamma_i = 1 - \frac{\Delta v_{1:i-1}}{\sqrt{\mu/r_0}} \tag{44}$$

and the initial angular position for each segment is defined recursively as

$$\theta_{0,i} = \begin{cases} \theta_0 & i = 1 \\ \theta_{i-1}(T_{i-1}) & i > 1 \end{cases} \tag{45}$$

IV. Sensitivity Approximation

Eqs. 39 and 43 give an approximation for the spacecraft's position in the orbital plane under the influence of a segmented along-track acceleration. The sensitivities required for the sensitivity matrix in Eq. 22 can be derived by taking the partial derivatives of Eqs. 39 and 43 with respect to each acceleration in the segment. Note that the trajectory approximation remains within a single orbit plane, therefore the derivative of the spacecraft's cross-track position with respect to any acceleration magnitude will be zero. Since the spacecraft position is given as a radial and angular position, the derivative in the along-track direction can be approximated as

$$\frac{\partial a}{\partial \alpha_i} \approx r_0 \frac{\partial \theta}{\partial \alpha_i} \tag{46}$$

Assume that the time of interest for calculating the sensitivity falls during segment i of the along-track acceleration profile. For the radial and angular positions, there are three derivative that need to be calculated. One derivative with respect to the acceleration of the current segment, α_i, another derivative with respect to the acceleration of previous segments, $\alpha_j, j < i$, and a final derivative with respect to the acceleration of future segments, $\alpha_j, j > i$. Since neither Eq. 39 nor Eq. 43 depend on the acceleration of future segments, the associated derivative will be zero in both cases.

Starting with the radial position, the derivative of the radial position with respect to the current acceleration, α_i, is given by

$$\frac{\partial}{\partial \alpha_i} r_i(t) = \frac{2r_0(t - T_{i-1})}{\sqrt{\mu/r_0}} \left(1 - \frac{\Delta v_{1:i-1}}{\sqrt{\mu/r_0}} - \frac{\alpha_i}{\sqrt{\mu/r_0}}(t - T_{i-1})\right)^{-3} \qquad t \in [T_{i-1}, T_{i-1} + \Delta t_i) \tag{47}$$

which can be closely approximated as

$$\frac{\partial}{\partial \alpha_i} r_i(t) \approx \frac{2r_0(t - T_{i-1})}{\sqrt{\mu/r_0}} \qquad t \in [T_{i-1}, T_{i-1} + \Delta t_i) \tag{48}$$

since in most practical cases, $\sqrt{\mu/r_0} \gg \Delta v_{1:i-1}$ and $\sqrt{\mu/r_0} \gg \alpha_i(t - T_{i-1})$. The derivative of the radial position with respect to any prior acceleration, $\alpha_j, j < i$, is given by

$$\frac{\partial}{\partial \alpha_j} r_i(t) = \left(\frac{\partial}{\partial \Delta v_{1:i-1}} r_i(t)\right)\left(\frac{\partial}{\partial \alpha_j} \Delta v_{1:i-1}\right) \tag{49}$$

$$= \frac{2r_0 \Delta t_j}{\sqrt{\mu/r_0}} \left(1 - \frac{\Delta v_{1:i-1}}{\sqrt{\mu/r_0}} - \frac{\alpha_i}{\sqrt{\mu/r_0}}(t - T_{i-1})\right)^{-3} \qquad t \in [T_{i-1}, T_{i-1} + \Delta t_i) \tag{50}$$

which can be closely approximated as

$$\frac{\partial}{\partial \alpha_j} r_i(t) \approx \frac{2r_0 \Delta t_j}{\sqrt{\mu/r_0}} \qquad t \in [T_{i-1}, T_{i-1} + \Delta t_i) \tag{51}$$

For the angular position, the derivative of the angular position with respect to the current acceleration, α_i, is given by

$$\frac{\partial}{\partial \alpha_i} \theta(t) = -\frac{1}{4r_0}(t - T_i)^2 \left[6\Gamma_i^2 - 8\Gamma_i \left(\frac{\alpha_i}{\sqrt{\mu/r_0}}(t - T_i)\right) + 3\left(\frac{\alpha_i}{\sqrt{\mu/r_0}}(t - T_i)\right)^2\right] \tag{52}$$

Under the assumption that $\sqrt{\mu/r_0} \gg \Delta v_{1:i-1}$ and $\sqrt{\mu/r_0} \gg \alpha_i(t - T_{i-1})$ then $\Gamma_i \approx 1$ and the derivative of the angular position with respect to the current acceleration can be approximated by

$$\frac{\partial}{\partial \alpha_i} \theta_i(t) \approx -\frac{3}{2}\frac{1}{r_0}(t - T_{i-1})^2 \qquad t \in [T_{i-1}, T_{i-1} + \Delta t_i) \tag{53}$$

The derivative of the angular position with respect to any prior acceleration, $\alpha_j, j < i$, is given by

$$\frac{\partial}{\partial \alpha_j} \theta_i(t) = \left(\frac{\partial}{\partial \Gamma_i} \theta_i(t)\right)\left(\frac{\partial}{\partial \Delta v_{1:i-1}} \Gamma_i\right)\left(\frac{\partial}{\partial \alpha_j} \Delta v_{1:i-1}\right) \tag{54}$$

$$= -\frac{1}{4r_0}\Delta t_j^2 \left[6\Gamma_j^2 - 8\Gamma_j \left(\frac{\alpha_i}{\sqrt{\mu/r_0}}\Delta t_j\right) + 3\left(\frac{\alpha_i}{\sqrt{\mu/r_0}}\Delta t_j\right)^2\right] - \frac{1}{r_0}\Delta t_j (t - T_i)\left[3\Gamma_i^2 - 3\Gamma_i \frac{\alpha_i}{v_0}(t - T_i) + \left(\frac{\alpha_i}{v_0}(t - T_i)\right)^2\right] \tag{55}$$

Under the assumption that $\sqrt{\mu/r_0} \gg \Delta v_{1:i-1}$ and $\sqrt{\mu/r_0} \gg \alpha_i(t - T_{i-1})$ then $\Gamma_j \approx \Gamma_i \approx 1$ and the derivative of the angular position with respect to any prior acceleration can be approximated by

$$\frac{\partial}{\partial \alpha_j}\theta(t) \approx -\frac{3\Delta t_j}{r_0}\left((t - T_{j-1}) - \frac{1}{2}\Delta t_j\right) \qquad t \in [T_{i-1}, T_{i-1} + \Delta t_i) \tag{56}$$

Given the approximate derivatives for the angular position, the derivatives for the along-track position can be calculated from Eq. 46. The derivative of the along-track position with respect to the current acceleration, α_i, can be approximated by

$$\frac{\partial}{\partial \alpha_i}a(t) \approx -\frac{3}{2}(t - T_{i-1})^2 \qquad t \in [T_{i-1}, T_{i-1} + \Delta t_i) \tag{57}$$

and the derivative of the along-track position with respect to any prior acceleration, α_j, $j < i$, can be approximated by

$$\frac{\partial}{\partial \alpha_j}a(t) \approx -3\Delta t_j\left((t - T_{j-1}) - \frac{1}{2}\Delta t_j\right) \qquad t \in [T_{i-1}, T_{i-1} + \Delta t_i) \tag{58}$$

Therefore, for a given measurement time, the sensitivities required for the sensitivity matrix in Eq. 22 can be calculated from Eqs. 48, 51, 57, and 58 depending on if the acceleration of interest is the acceleration of the current segment or was prior to the current segment. The sensitivities with respect to accelerations of future segments will always be zero.

Given the number of approximations taken to derive the above derivatives, it is worth comparing the analytical derivatives to numerically-determined derivatives. For the numerical comparison, the trajectory of a spacecraft initially in a 400 km altitude orbit about Earth is simulated with a 30th-order spherical-harmonics representation of the Earth's gravitational field using Joint Gravity Model 3 coefficients [28]. A five-segment piece-wise constant along-track acceleration is applied to the spacecraft with acceleration magnitudes for each segment randomized between -100–100 μm/s^2. The length of each segment is also randomized on the range 5–10 hours. 1000 samples were collected where for each sample the magnitude of a randomly-chosen acceleration was perturbed by a small acceleration on the range $\Delta\alpha \in [-10, 10]$ μm/s^2 and the change in the radial and along-track position of the spacecraft was then calculated at a randomly-chosen time. The nominal magnitudes and segment lengths for the accelerations were resampled between simulations.

Figure 1 shows the calculated deviations in the radial and along-track position of the spacecraft normalized by the analytically-derived derivatives in Eqs. 48, 51, 57, and 58 versus the applied deviations in the along-track acceleration magnitude. If the analytically-derived derivatives were accurate, then all of the samples should fall on a line of slope one. The samples do cluster around a line of slope one demonstrating that the analytically-derived derivatives do provide an accurate approximation of the actual sensitivities. This test was conducted using a relatively high-fidelity model—a 30th-order spherical-harmonics representation of the Earth's gravitational field—demonstrating that the derivatives would be accurate for most practical scenarios.

V. Maneuver Reconstruction

Given the analytical approximations for the sensitivities of radial and along-track deviations in the spacecraft's position, the process of maneuver reconstruction is relatively simple. For an assumed Gaussian prior distribution of the initial spacecraft state and magnitudes of each segment of the piece-wise constant along-track acceleration profile, first simulate the spacecraft's trajectory based on the mean values of each parameter and record the spacecraft's position at the desired measurement times. Given the simulated spacecraft position and the observed measurements, calculate the deviations of the observed measurements from the simulated spacecraft position in a local-vertical, local-horizontal plane in order to form the deviations in the alternate measurement vector in Eq. 18. In addition, determine the sensitivity matrix from Eq. 22 using the analytical sensitivities defined by Eqs. 48, 51, 57, and 58.

Given the measurement deviations and sensitivity matrix, determine the required shift in the mean values of the parameter vector according to Eq. 23, where initially $\Delta\bar{\phi} = 0$, as well as update the covariance of the parameter vector according to Eq. 24. After applying the shift in the mean values of the parameter vector, estimates for the initial spacecraft state as well as acceleration magnitudes for the piece-wise along-track acceleration profile conditioned on the observed measurements of the spacecraft state are obtained. In this approach it is additionally assumed that the simulation is free from model error and uncertainties in the initial spacecraft state and acceleration magnitudes will not include uncertainty due to potential model error.

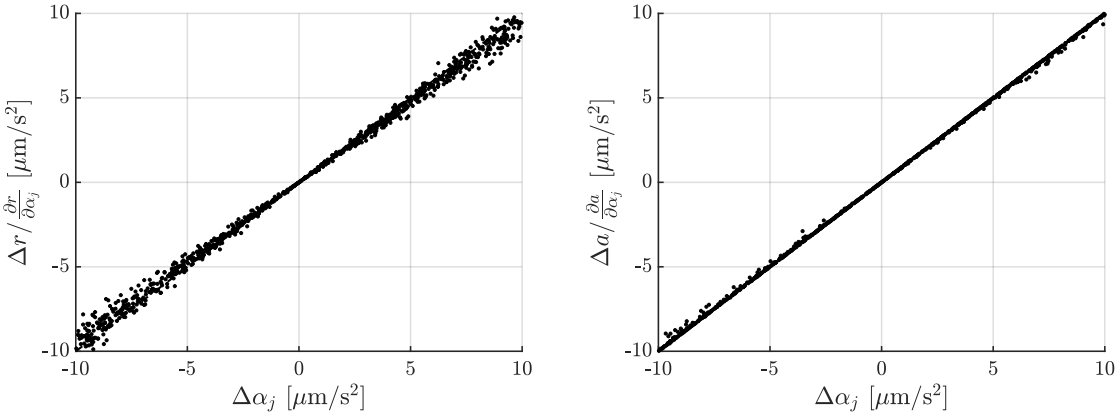

Fig. 1 Numerically-determined deviations in radial and along-track position normalized by the analytically-derived derivatives versus deviations in along-track acceleration magnitude.

VI. Applications

The maneuver reconstruction approach is quite general and can be applied to a number of applications. The following examples demonstrate the reconstruction of various maneuvers ranging from maneuvers with discontinuities in the acceleration profile—such as thruster startup—to smooth acceleration profiles—such as the degradation of a thruster over extended firing periods. In all cases a 30th-order spherical-harmonics representation of the Earth's gravitational field is used to simulate the measurements and the reference trajectory used for inference and the spacecraft is assumed to start in a 420 km altitude circular orbit around Earth. Note that due to the relatively low altitude of the spacecraft, the inferred acceleration can be inclusive of both atmospheric drag and propulsive accelerations. Measurements of the spacecraft's position are assumed to be independently distributed and to have a zero-mean Gaussian distribution with 3σ uncertainty of 100 m. The prior distributions for the initial spacecraft position and velocity are assumed to be independently distributed and zero-mean Gaussian distributions with 3σ uncertainties of 100 m and 1 m/s respectively. In the following examples, only the posterior distribution of the reconstructed acceleration profile is shown. The initial spacecraft state was also inferred, but is omitted here.

A. Discontinuous Profiles

Figure 2 shows the prior and posterior distributions of the reconstruction of an acceleration profile with a single discontinuity, perhaps representative of thruster startup. Error bars represent 3σ uncertainty in the segmented reconstruction. The true maneuver starts with an initial along-track acceleration of 0 μm/s^2 before increasing to 5 μm/s^2 2.5 hours later. The overall maneuver is assumed to take 10 hours with measurements collected once every minute. A ten-segment profile is used for the reconstruction where the prior distribution for the magnitude of each segment is assumed to be zero-mean Gaussian distributions with 3σ uncertainty of 10 μm/s^2. The posterior distributions of the acceleration magnitudes for the segmented profile demonstrate that the true acceleration profile is captured quite well. Of note is that the third segment is centered at 2.5 hour mark, where the true acceleration profile jumps from 0 μm/s^2 to 5 μm/s^2. The inferred magnitude for the acceleration of the third segment is close to 2.5 μm/s^2, representing the average acceleration of the true profile during the time period of the third segment. Across all segments, the posterior uncertainty in the acceleration magnitude has an average 3σ uncertainty of 1.7 μm/s^2 with a minimum of 1.0 μm/s^2 for the first segment and a maximum of 3.2 μm/s^2 for the final segment.

Figure 3 shows the prior and posterior distributions of the reconstruction of an acceleration profile with two discontinuities, perhaps representative of a maneuver detection scenario. Error bars represent 3σ uncertainty in the segmented reconstruction. The true maneuver starts with an initial along-track acceleration of 0 μm/s^2 before increasing to 5 μm/s^2 3.33 hours into the maneuver and then decreasing back to 0 μm/s^2 6.67 hours into the maneuver. As before, the overall maneuver is assumed to take 10 hours with measurements collected once every minute. A ten-segment profile is used for the reconstruction where the prior distribution for the magnitude of each segment is assumed to be zero-mean Gaussian distributions with 3σ uncertainty of 10 μm/s^2. The posterior distributions of the acceleration magnitudes for

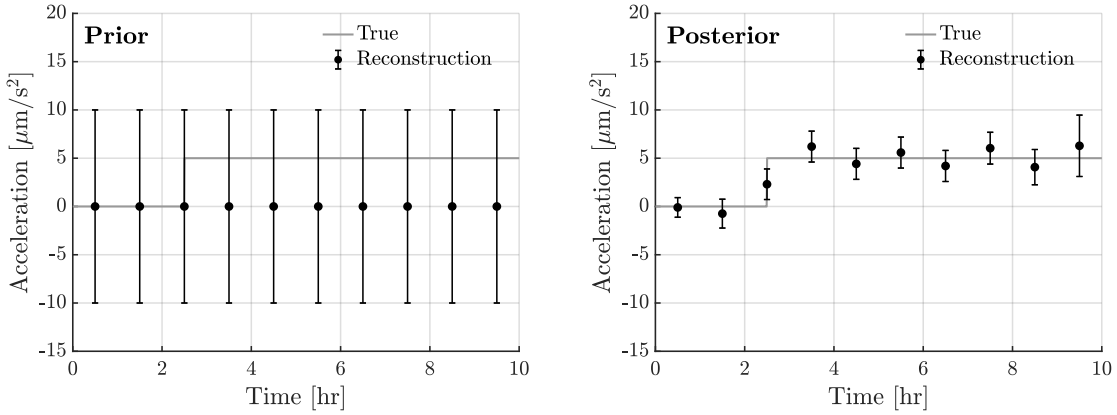

Fig. 2 Prior and posterior distributions of the along-track acceleration magnitudes when the true acceleration profile has a single discontinuity. Error bars represent 3σ uncertainty.

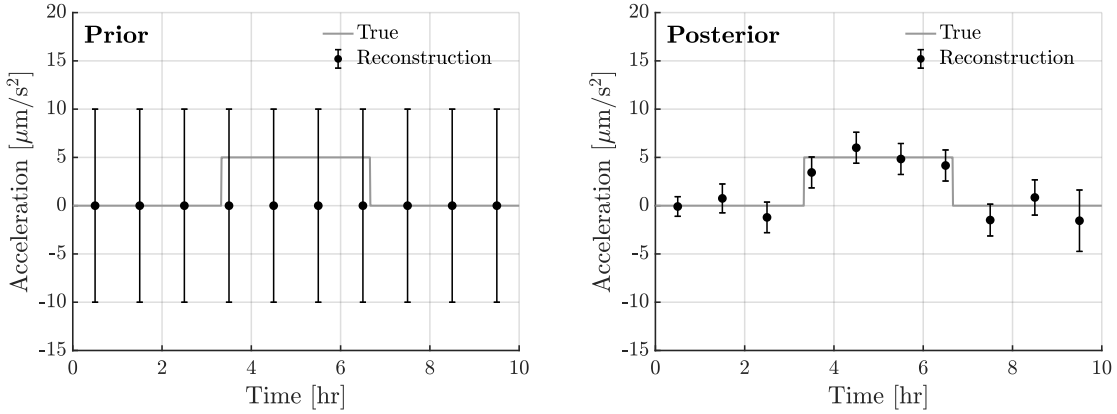

Fig. 3 Prior and posterior distributions of the along-track acceleration magnitudes when the true acceleration profile has two discontinuities. Error bars represent 3σ uncertainty.

the segmented profile again demonstrate that the true acceleration profile is captured quite well. In this profile, the true acceleration magnitude changes partially into the fourth segment and towards the end of the seventh segment of the segmented reconstruction. The primary impact of this is that the inferred magnitudes of the fourth and seventh segments are slightly lower than 5 μm/s^2 since the average true propulsive acceleration during both segments was slightly lower than 5 μm/s^2. A secondary impact is the the inferred magnitudes of the third and eighth segments are also lowered to accommodate for the fact that the reconstructed acceleration profile contains along-track acceleration in regions where the true acceleration is 0 μm/s^2. However, even despite this phenomena, detection of the maneuver is quite feasible based on the reconstructed acceleration profile. Since the prior uncertainties for this two-discontinuity profile are the same as in the one-discontinuity profile, the posterior uncertainties in the acceleration magnitudes are the same as before; across all segments, the posterior uncertainty in the acceleration magnitude has an average 3σ uncertainty of 1.7 μm/s^2 with a minimum of 1.0 μm/s^2 for the first segment and a maximum of 3.2 μm/s^2 for the final segment.

B. Continuous Profiles

Figure 4 shows the prior and posterior distributions of the reconstruction of an acceleration profile that is sinusoidal according to

$$\alpha_{\text{true}} = \alpha_0 \sin(\omega t) \tag{59}$$

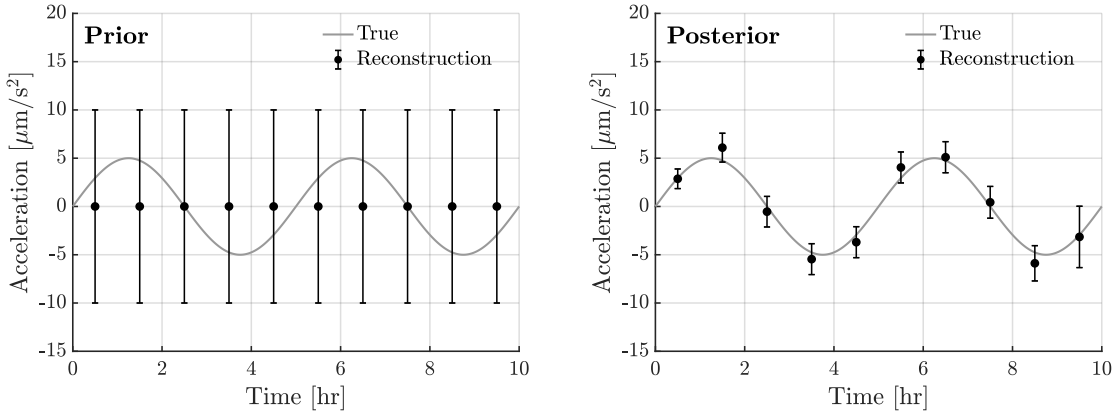

Fig. 4 Prior and posterior distributions of the along-track acceleration magnitudes when the true acceleration profile is sinusoidal. Error bars represent 3σ uncertainty.

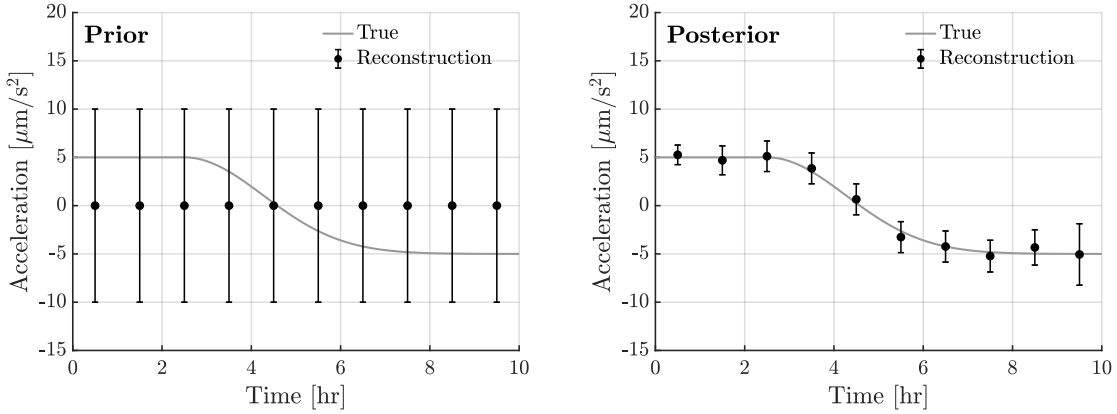

Fig. 5 Prior and posterior distributions of the along-track acceleration magnitudes when the true acceleration profile is an exponentiated quadratic. Error bars represent 3σ uncertainty.

where $\alpha_0 = 5$ μm/s^2 and $\omega = 0.4\pi$ 1/s. Error bars represent 3σ uncertainty in the segmented reconstruction. As before, the overall maneuver is assumed to take 10 hours with measurements collected once every minute. A ten-segment profile is used for the reconstruction where the prior distribution for the magnitude of each segment is assumed to be zero-mean Gaussian distributions with 3σ uncertainty of 10 μm/s^2. The posterior distributions of the acceleration magnitudes for the segmented profile reconstruct the sinusoidal profile by representing the approximate average value of the sinusoidal profile during each segment. Figure 5 shows the prior and posterior distributions of the reconstruction of an acceleration profile that is an exponentiated quadratic

$$\alpha_{\text{true}} = \begin{cases} \alpha_0 & t < T/4 \\ 2\alpha_0 \exp\left(-\left(\frac{t-T/4}{T/4}\right)^2\right) - \alpha_0 & t \geq T/4 \end{cases} \tag{60}$$

where $\alpha_0 = 5$ μm/s^2 and $T = 10$ hours. Error bars represent 3σ uncertainty in the segmented reconstruction. The overall maneuver length is kept at 10 hours and the measurement interval is still one minute. The same ten-segment prior profile is used as in the sinusoidal case. Again the continuous acceleration profile is represented quite well with the acceleration magnitude for each segment representing the approximate average value of the exponentiated quadratic profile during each segment.

As a practical example for the reconstruction of continuous along-track acceleration profiles, the case of reconstructing the approximate thrust decay of an electric propulsion system is considered. Electrospray thrusters have a thrust output

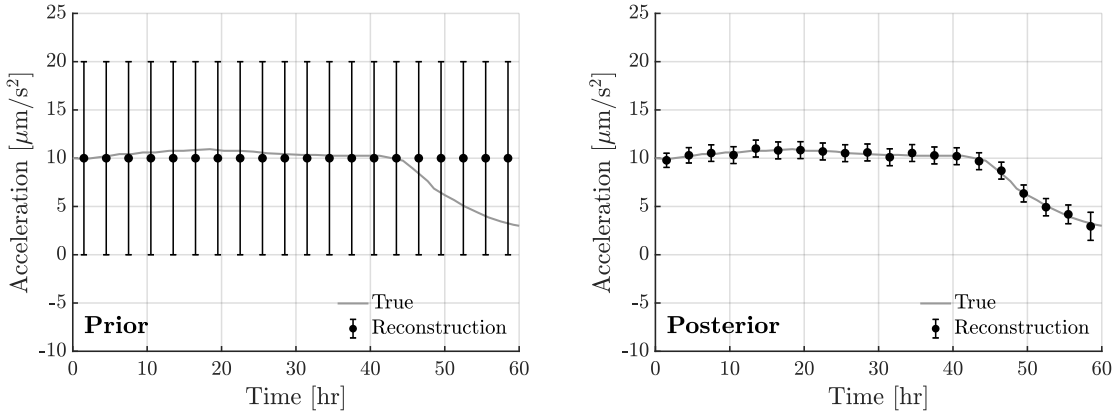

Fig. 6 Prior and posterior distributions of the along-track acceleration magnitudes when the true acceleration profile represents thruster degradation for an electrospray thruster. Error bars represent 3σ uncertainty.

that, to close approximation, is directly proportional to the emitted current for a constant thruster potential [29, 30]. By using experimental data for the emitted current of an electrospray thruster over time, a representative thrust—and therefore acceleration—profile can be obtained. Figure 6 shows the prior and posterior distributions of the reconstruction of an acceleration profile based on the emitted current profile of an electrospray thruster from Ref. [31]. Error bars represent 3σ uncertainty in the segmented reconstruction. Given a current profile, the acceleration profile is determined by scaling the current profile such that the initial acceleration is 10 μm/s^2. The variations in acceleration during the first 45 hours are caused by minor performance changes in the thruster over time. The drop in acceleration past 45 hours was caused by depletion of the propellant reservoir [31].

For the reconstruction of the acceleration profile, measurements were assumed to be collected once every hour. A twenty-segment profile is used for the reconstruction where the prior distribution for the magnitude of each segment is assumed to be a Gaussian distribution with mean of 10 μm/s^2 and 3σ uncertainty of 10 μm/s^2. The reconstructed profile is able to capture both the minor variations in propulsive acceleration during the first 45 hours as well as the steeper drop in acceleration past 45 hours due to propellant depletion. The average posterior 3σ uncertainty in the acceleration magnitude of the different segments was 0.90 μm/s^2. Such a technique could be used to characterize the long-term behavior of various low-thrust propulsion systems such as thrust degradation due to erosion in Hall thrusters [32] and pulsed-plasma thrusters [33]. While demonstrated here with electrospray thrusters, the method developed in this paper is propulsion system agnostic and can be used for any low-thrust propulsion system.

VII. Conclusion

This paper demonstrates that arbitrary acceleration profiles can be reconstructed through a piece-wise constant representation using analytical approximations for the sensitivity of a spacecraft's radial and along-track position with respect to the acceleration magnitude of each segment. Maneuver reconstruction was applied to both discontinuous and continuous acceleration profiles, including profiles based on the potential long-term variation in thrust of an electrospray thruster. The reconstructed acceleration profile was able to capture both minor variations in thrust during nominal thruster operation as well as more-rapid changes in thrust due to propellant depletion. Such a technique could be used to perform characterization of the long-term behavior of low-thrust propulsion systems.

The primary benefit of this work is that trajectories can be reconstructed with the simulation of only a single reference trajectory as opposed to the multiple simulations required for prior ensemble or iterative approaches. The use of only a single reference simulation dramatically reduces the computational cost of trajectory reconstruction, with the long-term goal of developing a method that could be implemented directly onto a spacecraft onboard computer for autonomous propulsion system characterization.

References

[1] Cybulski, R. J., Shellhammer, D. M., Lovell, R. R., Domino, E. J., and Kotnik, J. T., "Results from SERT I Ion Rocket Flight Test," Tech. rep., NASA, 1965.

[2] Kerslake, W. R., Goldman, R. G., and Nieberding, W. C., "SERT II: Mission, Thruster Performance, and In-Flight Thrust Measurements," *Journal of Spacecraft and Rockets*, Vol. 8, No. 3, 1971, pp. 213–224. https://doi.org/10.2514/3.30250.

[3] Sutton, E., Lin, C., Marcos, F., and Voss, D., "A CubeSat Constellation to Investigate the Atmospheric Drag Environment," *Proceedings of the Small Satellite Conference*, Utah State University, Logan, UT, USA, 2010.

[4] Young, B. and Martin-Mur, T., "Using Telemetry to Navigate the MarCO CubeSats to Mars," *Proceedings of the 18th Australian Aerospace Congress*, Melbourne, Australia, 2019.

[5] Rizvi, F., "Cassini Thruster Calibration Algorithm Using Reaction Wheel Biasing Data," *Journal of Spacecraft and Rockets*, Vol. 51, No. 2, 2014, pp. 563–573. https://doi.org/10.2514/1.A32523.

[6] Kramer, A., Bangert, P., and Schilling, K., "UWE-4: First Electric Propulsion on a 1U CubeSat—In-Orbit Experiments and Characterization," *Aerospace*, Vol. 7, No. 7: 98, 2020. https://doi.org/10.3390/aerospace7070098.

[7] Macario-Rojas, A. and Smith, K. L., "Spiral Coning Manoeuvre for In-orbit Low Thrust Characterisation in CubeSats," *Aerospace Science and Technology*, Vol. 71, 2017, pp. 337–346. https://doi.org/10.1016/j.ast.2017.09.035.

[8] Wiktor, P. J., "On-Orbit Thruster Calibration," *Journal of Guidance, Control, and Dynamics*, Vol. 19, No. 4, 1996, pp. 934–940. https://doi.org/10.2514/3.21721.

[9] Guerra-Garcia, C., Krejci, D., and Lozano, P., "Spatial Uniformity of the Current Emitted by an Array of Passively Fed Electrospray Porous Emitters," *Journal of Physics D: Applied Physics*, Vol. 49, No. 11, 2016, Paper 115503. https://doi.org/10.1088/0022-3727/49/11/115503.

[10] Chen, C., Chen, M., Fan, W., and Zhou, H., "Effects of Non-Uniform Operation of Emission Sites on Characteristics of a Porous Electrospray Thruster," *Acta Astronautica*, Vol. 178, 2021, pp. 192–202. https://doi.org/10.1016/j.actaastro.2020.09.002.

[11] Krejci, D., Mier-Hicks, F., Thomas, R., Haag, T., and Lozano, P. C., "Emission Characteristics of Passively Fed Electrospray Microthrusters with Propellant Reservoirs," *Journal of Spacecraft and Rockets*, Vol. 54, No. 2, 2017, pp. 447–458. https://doi.org/10.2514/1.A33531.

[12] Petro, E., Bruno, A., Lozano, P., Perna, L., and Freeman, D., "Characterization of the TILE Electrospray Emitters," *Proceedings of the AIAA Propulsion and Energy Forum*, Virtual Event, 2020. https://doi.org/10.2514/6.2020-3612.

[13] Pugia, S., Cofer, A., and Alexeenko, A., "Characterization of Film-Evaporating Microcapillaries for Water-Based Microthrusters," *Acta Astronautica*, Vol. 196, 2022, pp. 442–458. https://doi.org/10.1016/j.actaastro.2020.09.011.

[14] Samples, S. A. and Wirz, R. E., "Development of the MiXI Thruster with the ARCH Discharge," *Plasma Research Express*, Vol. 2, No. 2, 2020, p. 025008. https://doi.org/10.1088/2516-1067/ab906d.

[15] Krishnan, M., Velas, K., and Leemans, S., "Metal Plasma Thruster for Small Satellites," *Journal of Propulsion and Power*, Vol. 36, No. 4, 2020, pp. 535–539. https://doi.org/10.2514/1.B37603.

[16] Nakamura, T., Krech, R. H., and Smith, B. K., "Pulsed Electrogasdynamic Thruster for In-Space Propulsion," *Journal of Propulsion and Power*, Vol. 36, No. 6, 2020, pp. 950–960. https://doi.org/10.2514/1.B37298.

[17] Krejci, D., Reissner, A., Schönherr, T., Seifert, B., Saleem, Z., and Alejos, R., "Recent Flight Data from IFM Nano Thrusters in a Low-Earth Orbit," *Proceedings of the 36th International Electric Propulsion Conference*, Electric Rocket Propulsion Society, Vienna, Austria, 2019.

[18] Johnson, I. K., Santiago, G., Li, J., and Baldwin, J., "100,000hrs of On-Orbit Electric Propulsion and MAXAR's First Electric Orbit Raising," *Proceedings of the AIAA SciTech Forum*, American Institute of Aeronautics and Astronautics, Orlando, USA, 2020. https://doi.org/10.2514/6.2020-0189.

[19] Rafalskyi, D., Martínez Martínez, J., Habl, L., Zorzoli Rossi, E., Proynov, P., et al., "In-orbit Demonstration of an Iodine Electric Propulsion System," *Nature*, Vol. 599, 2021, pp. 411–415. https://doi.org/10.1038/s41586-021-04015-y.

[20] Goff, G. M., Black, J. T., and Beck, J. A., "Orbit Estimation of a Continuously Thrusting Spacecraft Using Variable Dimension Filters," *Journal of Guidance, Control, and Dynamics*, Vol. 38, No. 12, 2015, pp. 2407–2420. https://doi.org/10.2514/1.G001091.

[21] Guang, Z., Hanyu, Z., Qiuqiu, W., and Bin, L., "Relative Motion and Thrust Estimation of a Non-Cooperative Maneuvering Target with Adaptive Filter," *Acta Astronautica*, Vol. 162, 2019, pp. 98–108. https://doi.org/10.1016/j.actaastro.2019.05.032.

[22] Kelecy, T. and Jah, M., "Detection and Orbit Determination of a Satellite Executing Low Thrust Maneuvers," *Acta Astronautica*, Vol. 66, 2010, pp. 798–809. https://doi.org/10.1016/j.actaastro.2009.08.029.

[23] Qiao, J. and Chen, W., "Beidou Satellite Maneuver Thrust Force Estimation for Precise Orbit Determination," *GPS Solutions*, Vol. 22, No. 42, 2018. https://doi.org/10.1007/s10291-018-0705-2.

[24] Craft, K. J., Hecht, G. R., Darling, J. E., and Pernicka, H. J., "Development, Verification, and Analysis of a Small Satellite Thrust Determination Filter," *Journal of Spacecraft and Rockets*, Vol. 59, No. 2, 2022, pp. 360–374. https://doi.org/10.2514/1.A35147.

[25] Jia-Richards, O., Marzouk, Y., and Lozano, P., "A Method for Direct In-Space Thrust Estimation from Low-Acceleration Orbital Maneuvers," *Journal of Electric Propulsion*, Under review. https://doi.org/10.7302/7643.

[26] Prussing, J. E. and Conway, B. A., *Orbital Mechanics*, 2nd ed., Oxford University Press, New York, USA, 2012, pp. 179–188.

[27] Wiesel, W. E., *Spaceflight Dynamics*, 2nd ed., McGraw-Hill, New York, USA, 1997, pp. 90–92.

[28] Tapley, B. D. et al., "The Joint Gravity Model 3," *Journal of Geophysical Research*, Vol. 101, No. B12, 1996, pp. 28029–28049. https://doi.org/10.1029/96JB01645.

[29] Courtney, D., Dandavino, S., and Shea, H., "Comparing Direct and Indirect Thrust Measurements from Passively Fed Ionic Electrospray Thrusters," *Journal of Propulsion and Power*, Vol. 32, No. 2, 2016, pp. 392–407. https://doi.org/10.2514/1.B35836.

[30] Fedkiw, T., Wood, Z., Demmons, N., and Courtney, D., "Environmental and Lifetime Testing of the BET-300-P Electrospray Thruster," *AIAA Propulsion and Energy Forum*, American Institute of Aeronautics and Astronautics, Virtual Event, 2020. https://doi.org/10.2514/6.2020-3614.

[31] Krejci, D. and Lozano, P., "Micro-Machined Ionic Liquid Electrospray Thrusters for CubeSat Applications," *35th International Electric Propulsion Conference*, Electric Rocket Propulsion Society, Atlanta, USA, 2017.

[32] Brown, N. P. and Walker, M. L. R., "Review of Plasma-Induced Hall Thruster Erosion," *Applied Sciences*, Vol. 10, No. 11, 2020, p. 3775. https://doi.org/10.3390/app10113775.

[33] Krejci, D., Seifert, B., and Scharlemann, C., "Endurance Testing of a Pulsed Plasma Thruster for Nanosatellites," *Acta Astronautica*, Vol. 91, 2013, pp. 187–193. https://doi.org/10.1016/j.actaastro.2013.06.012.